Study of the wave damping, wave velocity and turbulence in an Artificial Rhizophora mangle Population (ARmP) including secondary roots.

Alejandra Piedrahita, Andrés Osorio, Liguia Urrego
{mapiedrahitao, afosorioar, leurrego}@unal.edu.co
Universidad Nacional de Colombia, Medellín, Colombia

Abstract. *Sea-level rise and extreme events, among many other problems, are the product of current human-caused climate change. The loss of some ecosystems, such as mangroves ecosystems, causes a rapid increase in the effects of climate change. Innovative studies on new uses for these forests can guarantee mechanisms for their conservation and protection. The objective of this research is to propose these forests as sediment retention and erosion control structures, through the study of wave velocity and turbulence between the roots of mangroves, these variables are related to sedimentation and erosion processes. A 1:10 scale physical model of an artificial Rhizophora mangle population (ARmP) exposed to oscillatory flow in the wave channel of the National University of Colombia - Medellín was made. The (ARmP) were parameterized in stainless steel considering the trunk and the primary and secondary roots. Eight wave gauges were implemented along the flume to record the free surface elevation and a 3-D Acoustic Doppler Velocimeter (ADV; Nortek Vectrino) were used to measured velocity profiles inside the model. A fixed wave height and depth H = 0.07 m, h = 0.28 m, and three wave period (T = 1 s, 1.2 s and 1.5 s), were considering. During the experiments, a 30% reduction in the stationary component of velocity within the (ARmP) regardless of the period, increase in velocities in high periods, negative Reynolds efforts, and wave damping 14 % were observed. Thus, it can be inferred this structure could be helpful in retain sediment and reducing erosional processes.*

Methodology

Design and scale to model mangrove forest.

For this study, an artificial Rhizophora mangle population (ARmP) was built on a 1:10 scale based on the Froude number. Primary and secondary roots were considered to try to simulate the aerial root system of these trees. For the design, the methodologies of Ohira et al. (2013) for the primary roots and (Järvelä, 2004) for the secondary roots were used.

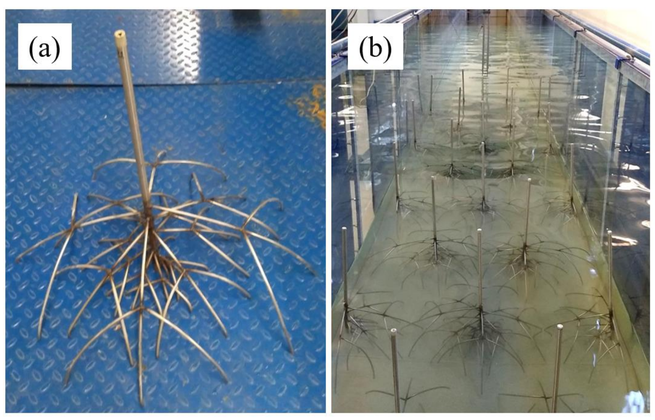

Figure 1. (a) Mangrove physical model in scale 1:10 (b) stepped arrangement of forests of mangrove models arranged within the channel.

Flume experiments.

- The wave parameters were selected considering the most frequent waves to which the mangroves are exposed under natural conditions and work intervals of the wavemaker system. Therefore, three cases were selected with a fixed wave height of H = 0.07 m, fixed depth of h = 0.28 m, and three periods (T = 1 s, 1.2 s and 1.5 s).
- The experiments were made in the wave channel of the hydraulics laboratory of the National University of Colombia, Medellín, with dimensions of 25 m long, 1 m wide and 1 m high.
- To dissipate the waves, we installed a beach of nylon foam with a 1:5 slope superimposed on a gravel beach at the opposite end of the channel, producing a reflection percentage between 2% and 20%, depending on the wave parameter.
- The mangrove forest was located in the middle of the channel to avoid contamination of the wave product of the reflection of the wavemaker and the beach.
- The velocity profiles were measured using an Acoustic Doppler Velocimeter 3D (ADV, Nortek Vectrino) placed in two different positions.
- Wave height were taken by of 8 resistive sensors with fixed carbon-type resistance of the HR Wallingford brand, distributed along the channel

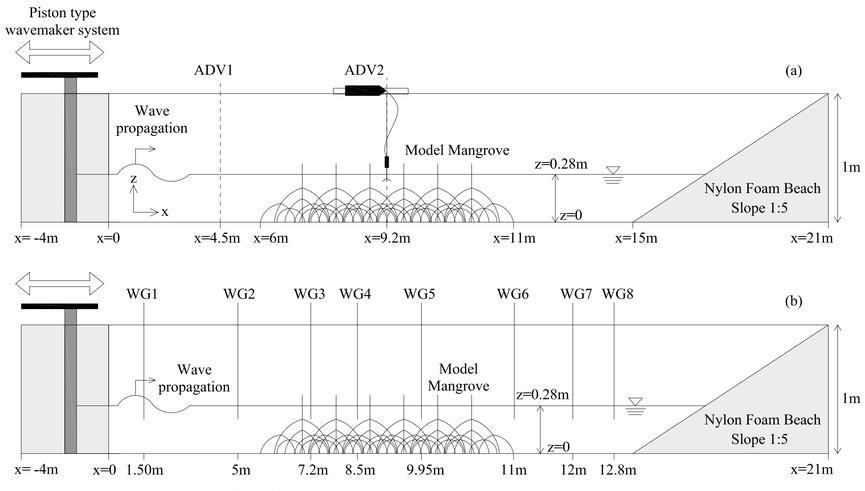

Figure 2. Experimental setup for (a) velocity measurements, the bold dashed line indicates measurement locations for vertical profile and (b) wave decay measurement, the solid line represents the wave gauges along the model canopy. Dimensions are in meter but not to scale

Equations.

- By of the threshold phase space method proposed by Goring and Nikora (2002) we eliminating the noise of the signal and the spikes.
- We determined the three components of the velocity obtained with the ADV by using the technique of the average phase, using by (Luhar et al., 2010; Pujol et al., 2013; Zhang et al., 2018)

U_i is the instantaneous velocity (Zhang et al., 2018).	$U_i = U_c + U_w + u'$
Uc is the steady component velocity (Zhang et al., 2018).	$U_c = \frac{1}{N_p}\int_0^{N_p} U_i\, dn$
$U_{w,RMS}$ is the standard deviation or the root-mean-square (rms) of the fluctuation, in this case the oscillatory wave component. That show the magnitude of this component. (Zhang et al., 2018).	$U_{w,rms} = \sqrt{\frac{1}{2\pi}\int_0^{2\pi} (\overline{U_i}(\varphi) - U_c)^2\, d\varphi}$
u'_{rms} is the standard deviation or the root-mean-square (rms) of the fluctuation, in this case the turbulence component. That show the magnitude of this component.	$u'_{rms}(\varphi) = \int_0^{N_p}\left(\sqrt{\frac{1}{2\pi}\int_0^{2\pi}(U_i - U_c - U_w)^2\, d\varphi}\right) dn$
TKE is the turbulent kinetic energy (Zhang and Nepf, 2019).	$TKE = \frac{1}{4\pi}\int_0^{2\pi}[u'_{rms}(\varphi)^2 + v'_{rms}(\varphi)^2 + w'_{rms}(\varphi)^2]\, d\varphi$
$\overline{u'w'}$ is the Reynolds stress (Zhang and Nepf, 2019).	$\overline{u'w'} = \frac{1}{2\pi}\frac{1}{N_p}\int_0^{2\pi}\int_0^{N_p} u'(\varphi,n)w'(\varphi,n)\, dnd\varphi$

Results and discussions.

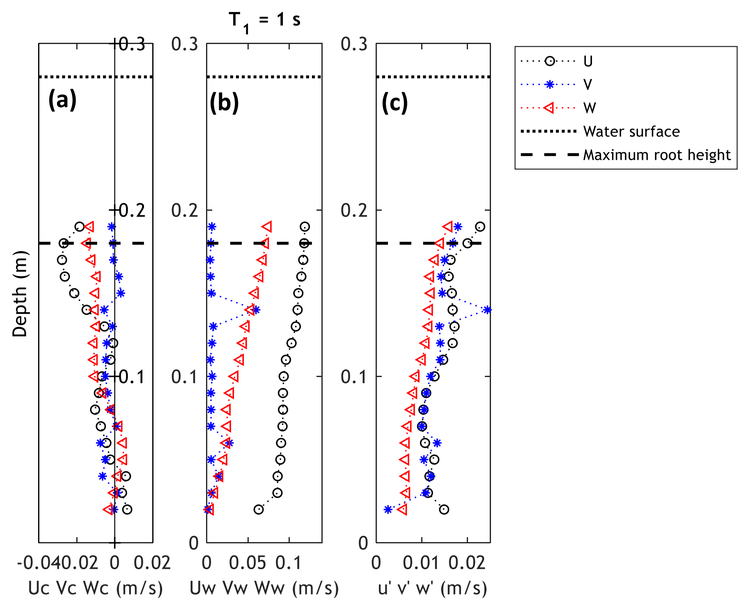

Figure 3. Magnitudes for the components velocities for the X (U-In the direction of the wave), Y (V-Transversal to channel) and Z (W-Vertical) axis for H = 0.07 m, T= 1 s and h=0.28 m with mangrove model. (a) The steady component velocity. (b) The root-mean-square (rms) of the oscillatory component. (c) The root-mean-square (rms) of the turbulence component.

- The behavior of the magnitude of the three components of velocity for the cases T = 1.2 s and T = 1.5 s was similar to that shown in Figure 3 for a T = 1 s. An increase in the magnitudes was evidenced, according to the increase in the period.
- The stationary component (Figure 3 - a) of the velocity in the x-axis, presents a greater magnitude of the three components, followed by the component in z and finally the component in the y-axis presents the smallest magnitude of the three components.
- Negative values of the stationary component are associated with return currents present in the wave channel.
- The magnitude of the oscillatory component (Figure 3 - b) was greater for the X axis, followed by the Z axis, and the axis that shows the lowest magnitude is the Y axis (transversal to the channel).
- The magnitude of the turbulent component (Figure 3 - c) was greater for the X (U-In the direction of the wave) and Y (V-Transversal to channel) axes. A lower magnitude was observed for the Z axis (W-Vertical).

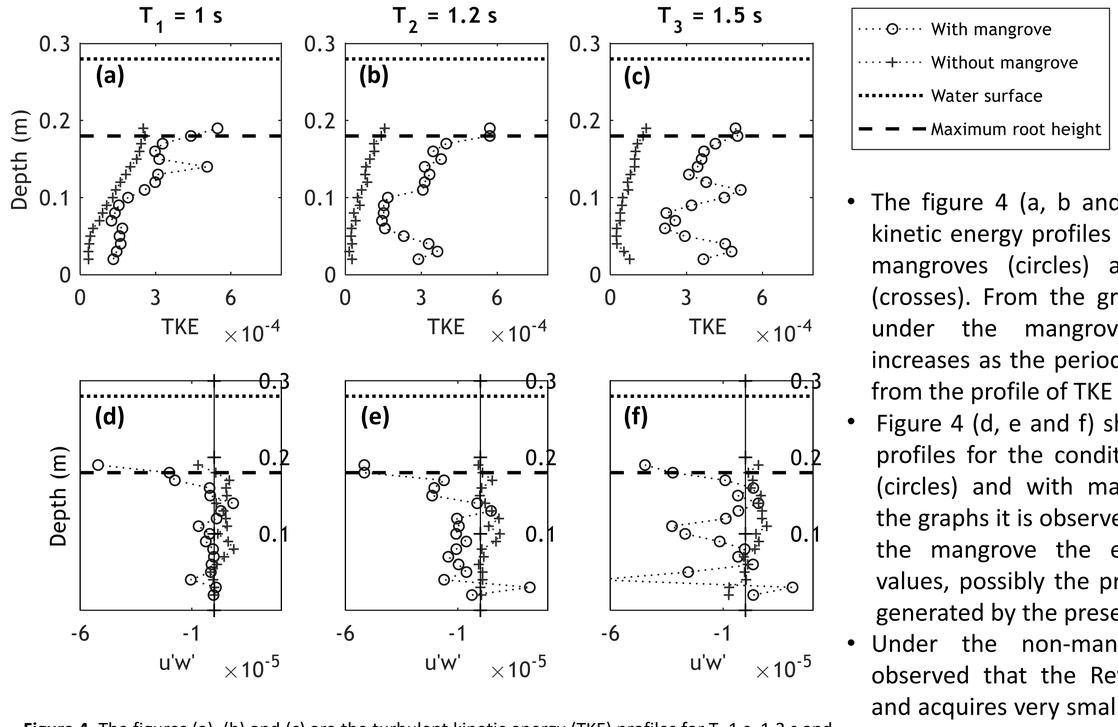

Figure 4. The figures (a), (b) and (c) are the turbulent kinetic energy (TKE) profiles for T=1 s, 1.2 s and 1.5 s respectively. The figures (d), (e) and (f) are the Reynolds stress profiles for T=1 s, 1.2 s and 1.5 s respectively. The circles represent the mangrove condition, the crosses are the non-mangrove condition, the dotted line is the water surface and the dashed line shows the maximum root height.

- The figure 4 (a, b and c) shows the turbulent kinetic energy profiles (TKE) for conditions with mangroves (circles) and without mangroves (crosses). From the graphs it is observed that under the mangrove condition the TKE increases as the period increases, moving away from the profile of TKE without mangrove.
- Figure 4 (d, e and f) shows the Reynolds stress profiles for the conditions without mangroves (circles) and with mangroves (crosses). From the graphs it is observed that in the presence of the mangrove the effort acquires negative values, possibly the product of return currents generated by the presence of the mangrove.
- Under the non-mangrove condition, it is observed that the Reynolds stress is positive and acquires very small values, compared to the mangrove condition. It is also observed that the Reynolds stress under the mangrove condition increases as the period increases.

Conclusions

- According to the results, the negative Reynolds stress appears in areas with currents in the opposite direction to the direction of wave propagation, as seen in Figure 3 (a). Therefore, these currents appear to be associated with the presence of the mangrove and their effects increase as the period increases. This same result is described in similar laboratory studies conducted by Zhang and Lai, 2015.

- The Reynolds stress with waves and without mangroves is positive and takes values close to zero, similar to the result shown by Umeyama, 2005.

References

Goring, D.G., Nikora, V.I., 2002. Despiking Acoustic Doppler Velocimeter Data. Journal of Hydraulic Engineering 128, 117–126. https://doi.org/10.1061/(ASCE)0733-9429(2002)128:1(117)

Järvelä, J., 2004. Determination of flow resistance caused by non-submerged woody vegetation. International Journal of River Basin Management 2, 61–70. https://doi.org/10.1080/15715124.2004.9635222

Luhar, M., Coutu, S., Infantes, E., Fox, S., Nepf, H., 2010. Wave-induced velocities inside a model seagrass bed. Journal of Geophysical Research 115. https://doi.org/10.1029/2010JC006345

Ohira, W., Honda, K., Nagai, M., Ratanasuwan, A., 2013. Mangrove stilt root morphology modeling for estimating hydraulic drag in tsunami inundation simulation. Trees 27, 141–148. https://doi.org/10.1007/s00468-012-0782-8

Pujol, D., Serra, T., Colomer, J., Casamitjana, X., 2013. Flow structure in canopy models dominated by progressive waves. Journal of Hydrology 486, 281–292. https://doi.org/10.1016/j.jhydrol.2013.01.024

Umeyama, M., 2005. Reynolds Stresses and Velocity Distributions in a Wave-Current Coexisting Environment. J. Waterway, Port, Coastal, Ocean Eng. 131, 203–212. https://doi.org/10.1061/(ASCE)0733-950X(2005)131:5(203)

Zhang, X., Chua, V.P., Cheong, H.-F., 2015. Hydrodynamics in mangrove prop roots and their physical properties. Journal of Hydro-environment Research 9, 281–294. https://doi.org/10.1016/j.jher.2014.07.010

Zhang, Y., Nepf, H., 2019. Wave-Driven Sediment Resuspension Within a Model Eelgrass Meadow. J. Geophys. Res. Earth Surf. 124, 1035–1053. https://doi.org/10.1029/2018JF004984

Zhang, Y., Tang, C., Nepf, H., 2018. Turbulent Kinetic Energy in Submerged Model Canopies Under Oscillatory Flow. Water Resources Research 54, 1734–1750. https://doi.org/10.1002/2017WR021732